Redistribution of REE, Pb and U by supergene weathering studied from *in-situ* isotopic analyses of the Bangombé natural reactor, Gabon

M. Kikuchi,[1] H. Hidaka,[1,2]* K. Horie,[1,3] and F. Gauthier-Lafaye[2]

[1]Department of Earth and Planetary Systems Science, Hiroshima University, Higashi-Hiroshima 739-8526, Japan

[2]Centre de Geochimie de la Surface, Ecole et Observatoire des Sciences de la Terre, UMR7517-CNRS-ULP, 1 rue Blessig, 67084 Strasbourg, France

[3]Department of Science and Engineering, National Science Museum, Tokyo 169-0073, Japan

*Author to whom correspondence should be addressed (hidaka@hiroshima-u.ac.jp)

Abstract

The isotopic analyses of rare earth elements (REE), Pb and U in several kinds of minerals from the clay and black shale layers above the Bangombé natural reactor, Gabon, were performed using a sensitive high resolution microprobe (SHRIMP) to investigate the migration and retardation processes of fission products released from the reactor. REE isotopic data of the secondary minerals found in clays and black shales show that most of fission products were effectively trapped in the clays and not distributed into the black shales over the clays, which reveals that the clays play an important role in preventing fission products from spreading.

Zircon crystals in the clays heterogeneously contain high-U regions (up to 28.3 wt.%) with normal $^{235}U/^{238}U$ ratios (=0.00725) and significant amounts of fissiogenic REE, which suggests the occurrence of significant chemical fractionation between REE and U during the dissolution of reactor uraninite and the recrystallization of secondary U minerals. The Pb data suggest that galena grains in the clays were also formed by the mixing of the two components during a recent alteration event, and that a significant amount of Pb was derived from 2.05-Ga-old original uraninite rather than reactor uraninite. The U-Pb systematics of zircon provide chronological information on the old igneous activity associated with the basement rock formation at 2.8 Ga and geochemical evidence of the incomplete mixing of independent Pb and U sources. This result is consistent with previous chronological results in this area.

1. Introduction

The Oklo-Okélobondo-Bangombé uranium deposits in the Republic of Gabon, central Africa, are known as natural fission reactors. Large-scale fission chain reactions spontaneously occurred at 16 separate areas in the Oklo deposit, so-called "reactor zones (hereafter RZs)", approximately 2.0 Ga ago, and sustained for 24000 to 200000 years (Gauthier-Lafaye et al., 1996). Two more RZs have been identified at the Okelobondo and Bangombé uranium deposits close to Oklo. The deposition age of primary uraninite in this area was dated as 2.05 ± 0.03 Ga by Gancarz (1978). On the other hand, reactor uraninite also yielded similar ages, 1.97 ± 0.06 Ga (Gancarz, 1978), 1.97 ± 0.05 Ga (Holliger, 1988) and 2.02 ± 0.03 Ga (Gauthier-Lafaye et al., 1996). Therefore, considering the analytical uncertainties, it is difficult to distinguish the age differences between these two events.

Many elements consisting of the reactor samples show variable isotopic compositions due to nuclear fission and neutron capture reactions. Therefore, isotopic studies of the reactor materials provide practical information on the long-term behavior of fission products in geological media, which is applicable to radioactive waste disposal (e.g., Gauthier-Lafaye et al., 1996; Hidaka and Holliger, 1998). Most of previous isotopic analyses in Oklo studies were based on the bulk analysis of whole rock samples with the chemical separation of individual elements for the determination of their isotopic compositions using thermal ionization mass spectrometry (TIMS) and inductively coupled plasma mass spectrometry (ICP-MS). Although such bulk analyses have provided precise isotopic data, the results indicate average information on isotopes in the samples. Isotopic information from microscopic regions is essential for further discussion and understanding of the detailed processes of the migration and

fixation of fission products.

Mineralogical observations have shown the existence of tiny secondary minerals in alteration phases around the reactors in association with the partial dissolution of the reactor uraninite, suggesting the precipitation of fission products migrated from the reactor (Janeczek and Ewing, 1996a; Jensen and Ewing, 2001). However, the interpretation was not supported by isotopic data. To address this issue, *in-situ* isotopic analyses of the micro-minerals found in the peripheral rocks of the reactors have been performed by secondary ion mass spectrometry (SIMS) (Janeczek and Ewing, 1996b; Bros et al., 2003; Horie et al., 2004; Hidaka et al., 2005). SIMS has been widely applied for the *in-situ* isotopic analyses of geological samples for two decades. *In-situ* isotopic analyses of individual minerals using SIMS provide information on the detailed thermal history of geological materials.

The Bangombé RZ is located at 11.80 m depth within the groundwater discharge area, and is significantly affected by weathering and chemical reactions due to the flow of groundwater. In addition, the intrusion of numerous dolerite dykes were caused by regional extension in the Franceville basin, which was confirmed as several episodes of significant Pb mobilization in Late Proterozoic period (Gauthier-Lafaye et al., 1996). This suggests that a part of the fission products have been released from the reactor and distributed in the peripheral rocks. The migration behavior of fissiogenic REE can be discussed from the distribution profile of isotopic variations with the distance from the RZ. In early research, the isotopic data of the Bangombé site suggested that the fission products released from the RZ during recent weathering have been distributed over a distance of 1 m into a sandstone beneath the RZ (Hidaka et al., 2005), but have been retained in a clay layer above the RZ (Stille et al., 2003).

The isotopic analyses of lighter REE (LREE) in micro-regions using SIMS have been effectively used to discuss the migration processes of fissiogenic isotopes into U- and REE-bearing minerals, because a large amount of LREE is produced by U fission in natural reactors. Several kinds of secondarily formed U- and REE-bearing minerals such as florencite and coffinite have been found in the peripheral rocks of the RZ (Janeczek and Ewing, 1996a). The phosphate minerals found in the host rock contain an excess of fissiogenic LREE (Janeczek and Ewing 1996b; Dymkov et al., 1997; Hidaka et al., 2005), which suggests that the large amount of LREE in the RZ was released in association with the alteration of the reactor uraninite and precipitated as phosphate minerals. Our major concern is when and how fission products were released from the reactor and trapped in the individual minerals. In this paper, we report the LREE isotopic data of several kinds of micro-minerals found in the peripheral rocks of the Bangombé RZ and then discuss the mechanisms of mobilization and retardation of fissiogenic isotopes produced in the RZ. Furthermore, a chronological interpretation of the timing of LREE migration in association with the geological events around this site is deduced from the U and Pb isotopic data of the U and Pb minerals.

2. Experimental procedures

2.1. Samples

The Bangombé uranium deposit is located approximately 30 km southeast from the Oklo-Okelobondo uranium deposits. Figure 1 shows a map of the Bangombé site with the location of the RZ and the main boreholes. More than twenty boreholes have been drilled to investigate the geological setting of the Bangombé RZ, but only three boreholes (BA145, BAX3 and BAX8) intersect the RZ (Gauthier-Lafaye et al.,

1996; Hidaka and Holliger, 1998). Stille et al. (2003) reported the isotopic variations of $^{143}Nd/^{146}Nd$ and $^{149}Sm/^{147}Sm$ in one of the drill cores BAX8, including the RZ, and concluded that fissiogenic REE were not detected at a distance of more than 3 m from the reactor. Therefore, in this study, we focused on the region within 1 m above and beneath the reactor.

In our previous study, four samples, BAX3.1215, 1225, 1240 and 1290, from the sandstone layer beneath the RZ were used. The LREE isotopic data showed that the proportion of fissiogenic and non-fissiogenic REE components gradually change with the distance from the RZ (Hidaka et al., 2005). Three samples, BAX3.1040, 1065 and 1170, used in this study were collected from BAX3. The sub-number (four digits) of each sample corresponds to its depth in the BAX3 borehole in cm. The reactor part of Bangombé corresponds to BAX3.1180. BAX.3.1170 consists of clays from 10 cm above the reactor. BAX3.1040 and 1065 are black shales taken from 140 and 115 cm above the RZ, respectively. The black shales include fine fractures filled with iron and manganese oxides. The petrologic stratigraphic section of the BAX3 drilling-core is shown in Fig. 2.

2.2. Analytical methods

Each sample was cut and mounted in an epoxy resin disk of 2.5 cm diameter. The surface of the sample was polished with 1/4 μm diamond paste. Before *in-situ* isotopic analyses, mineral observations of the polished sections of the samples were carried out using an optical microscope and an electron probe micro-analyzer (EPMA: JEOL XA-8200).

A Sensitive High Resolution Ion Micro-Probe (SHRIMP II) was used for

in-situ isotopic analyses in this study. For the REE measurements, the mass resolution was set to higher than 8800 (M/ΔM at 1% of peak height) to avoid the isobaric interferences of the oxide and unknown species onto atomic REE ion peak. The masses of ^{140}Ce, ^{142}Ce+^{142}Nd, ^{143}Nd, ^{144}Sm+^{144}Nd, ^{145}Nd, ^{146}Nd, ^{147}Sm, ^{148}Nd, ^{149}Sm, ^{150}Nd+^{150}Sm, ^{151}Eu, ^{152}Sm, ^{153}Eu, ^{155}Gd, ^{156}Gd+^{156}Dy, ^{157}Gd, ^{158}Gd+^{158}Dy, ^{160}Gd+^{160}Dy, and ^{161}Dy were scanned for the isotopic analyses. ^{142}Ce, ^{144}Sm and ^{150}Sm isotopic abundances can be obtained from the subtraction of the ^{142}Nd, ^{144}Nd and ^{150}Nd isotopic abundances, respectively, because the isotopic abundances of ^{142}Nd, ^{144}Nd, and ^{150}Nd can be predicted from those of ^{145}Nd, ^{146}Nd and ^{148}Nd (Hidaka et al., 2005). Similarly, ^{156}Gd, ^{158}Gd and ^{160}Gd isotopic abundances were calculated after the subtraction of the isobaric interference of the Dy isotopes from the ^{161}Dy isotopic abundance, although the isotopic abundances of ^{156}Dy, ^{158}Dy and ^{160}Dy were negligibly low (Horie et al., 2004).

For the Pb isotopic analysis of galena, the masses of ^{204}Pb, ^{206}Pb, ^{207}Pb and ^{208}Pb were scanned with a mass resolution of 5800. For U-Pb analyses of zircon, $^{196}Zr_2O$, ^{204}Pb, ^{206}Pb, ^{207}Pb, ^{208}Pb, ^{238}U, ^{248}ThO and ^{254}UO peaks were measured with a mass resolution of 5800. For the U-Pb data calibation of zircon samples, FC1 (^{206}Pb/^{238}U=0.1859, 1099 Ma) was used as a standard material (Paces and Miller, 1993). In addition, SL13 (U content=238 ppm) was also used as a standard material for the determination of U concentration.

3. Results and discussion

3.1. REE distribution in U-bearing minerals

Isotopic and chemical analyses of whole rock samples from the Bangombé RZ apparently show that fissiogenic REE have been well-preserved in the RZ (Hidaka and

Gauthier-Lafaye, 2000). However, from a microscopic viewpoint, a trace of fissiogenic REE was released from the RZ in association with the partial dissolution of the reactor uraninite, and formed secondary minerals in the peripheral rocks. As REE-enriched minerals, apatite, monazite, florencite, rhabdophane, crandallite and françoisite have been found in the sandstones and clays near the Bangombé RZ (Janeczek and Ewing, 1996a; 1996b; Stille et al., 2003; Hidaka et al., 2005). In this study, coffinite, françoisite, U-rich inclusions coexisting with galena, and zircon were found in the clays. On the other hand, no REE minerals of over 1 μm-length were found in the black shales of the drill-core. Only uranium-rich phases of less than 1 μm (hereafter micro-uraninite) were included in the matrices of the black shales. Back-scattered electron (BSE) images of typical U- and REE-bearing minerals measured in this study are shown in Figs. 3 (A) to (D). Besides the U- and REE-bearing minerals, number of fine galena grains (Fig. 3(E) as a typical example) and seven zircon crystals (Fig. 3(F)) were also found in the clay.

The isotopic analyses of LREE are important for knowing the mobility of REE in association with the alteration of uraninite. The REE isotopic ratios of the individual minerals found in the clays (BAX3.1170) and those of the micro-uraninite in the black shales (BAX3.1065 and 1040) are listed in Table 1. Fission and neutron capture are main reactions that cause the significant isotopic anomalies of the elements in a natural reactor. The ^{140}Ce, ^{142}Ce, ^{143}Nd, ^{146}Nd, ^{147}Sm, ^{149}Sm, ^{151}Eu and ^{153}Eu isotopes of the samples measured in this study include the fissiogenic component as well as the non fissiogenic component, because they are not shielded by β^- decay. Considering the fission product yields of individual isotopes, the ^{140}Ce/^{142}Ce isotopic ratios of the samples are expected to be lower than those of the non fissiogenic standard

sample ($^{140}Ce/^{142}Ce=7.73 \pm 0.03$). On the other hand, the $^{143}Nd/^{146}Nd$ and $^{151}Eu/^{153}Eu$ isotopic ratios of the samples are expected to be higher than those of the standard samples ($^{143}Nd/^{146}Nd=0.735 \pm 0.01$ and $^{151}Eu/^{153}Eu=1.092 \pm 0.002$). The $^{149}Sm/^{147}Sm$ ratios are expected to be lower than those of the standard materials ($^{149}Sm/^{147}Sm=0.906 \pm 0.001$) because of the extremely large neutron capture cross section of ^{149}Sm.

The most important difference in mineralogy between BAX3 and the other drill cores is the occurrence of uraninite with coffinite and phosphatian U-minerals. The coffinite and posphatian minerals are considered to be formed by supergene weathering (Stille et al., 2003; Gauthier-Lafaye et al., 2004). The isotopic data of $^{140}Ce/^{142}Ce$, $^{143}Nd/^{146}Nd$ and $^{149}Sm/^{147}Sm$ show clear evidence of the incorporation of fissiogenic isotopes in the minerals, while those of $^{151}Eu/^{153}Eu$ are unclear because of the low fission-product yields of ^{151}Eu and ^{153}Eu. The isotopic variations of $^{140}Ce/^{142}Ce$, $^{143}Nd/^{146}Nd$ and $^{149}Sm/^{147}Sm$ values depend upon the proportion of the fissiogenic component relative to the total fraction of individual minerals.

Figure 4 shows the depth-dependent variations of $^{140}Ce/^{142}Ce$, $^{145}Nd/^{146}Nd$, $^{149}Sm/^{147}Sm$ and $^{153}Eu/^{151}Eu$ isotopic ratios of U-bearing minerals in the BAX3 drill core. The isotopic data from previous works are also plotted in the same figure (Janeczek and Ewing, 1996b; Hidaka and Gauthier-Lafaye, 2000; Hidaka et al., 2005). The vicinity of the RZ, corresponding to BAX3.1180, has the lowest $^{140}Ce/^{142}Ce$ (2.209) and $^{149}Sm/^{147}Sm$ (0.1010) values and the highest $^{145}Nd/^{146}Nd$ (1.025) and $^{153}Eu/^{151}Eu$ (1.230) values, as shown in Table 1(A). These isotopic ratios gradually change with the distance from the reactor in the sandstone layer (1215 to 1290), which reveals that supergene weathering led to the redistribution of fissiogenic REE. However, the variations of the isotopic ratios above the RZ (BAX3.1050 to 1180) are different from

those under the RZ.

The isotopic variations of Ce, Nd and Sm in the clay layer (BAX3.1170) are much larger than those in the sandstones (BAX3.1225, 1240 and 1290) and black shales (BAX3.1040 and 1065), which indicates that the migration of fissiogenic LREE was limited. The variations of the isotopic ratios of REE drastically change in the clay, while the isotopic ratios gradually change with the distance from the reactor in the sandstone. Our isotopic data suggest that most of the fissiogenic Ce, Nd and Sm were effectively trapped in the clays, and not moved to the blackshales. This result provides a practical illustration of the performance of a clay barrier in the uptake of fission products by adsorption onto clays and their incorporation in secondarily formed U- and REE-bearing minerals.

Gd isotopic compositions are strongly affected by neutron capture reactions, because ^{155}Gd and ^{157}Gd have large neutron-capture cross sections and become ^{156}Gd and ^{158}Gd, respectively (Hidaka and Masuda, 1988; Hidaka and Holliger. 1998; Horie et al., 2004). Therefore, the isotopic depletion of ^{155}Gd and ^{157}Gd corresponds to the enrichment of ^{156}Gd and ^{158}Gd, respectively. If the Gd isotopic compositions of the samples are affected by only neutron-capture reactions, the isotopic ratios (^{155}Gd+^{156}Gd)/^{160}Gd and (^{157}Gd+^{158}Gd)/^{160}Gd should be constant because of the isotopic balance between the depletion of ^{155}Gd and ^{157}Gd and the enrichment of ^{156}Gd and ^{158}Gd. As shown in Table 1(B), the ratios of both (^{155}Gd+^{156}Gd)/^{160}Gd and (^{157}Gd+^{158}Gd)/^{160}Gd for coffinite-1 to coffinite-3 grains are in good agreement with those of the standard material within analytical precision. However, the corresponding isotopic ratios of coffinite-4 and the U-rich inclusion are 5-7 % higher than those in the standard material, which reveals isotopic evidence of the addition of a fissiogenic Gd

component as well as neutron-capture products in the samples.

3.2. Pb isotopic evolution of galena

Although the chronological interpretation of U-Pb and Pb-Pb data from the Oklo and Bangombé samples is often complicated because of the significant mobilization of Pb due to later igneous events (Gauthier-Lafaye et al., 1996), detailed comparison of the Pb isotopic data makes it possible to discuss the alteration history of the Oklo and Bangombé sites since the deposition of uranium ores (Mathieu et al., 2001; Evins et al., 2005; Hidaka et al., 2005). The Pb isotopic data of galena in the clay sample (BAX3.1160) are listed in Table 2. The variation of $^{207}Pb/^{206}Pb$ (0.1157 to 0.1362) is small and correlates with that of $^{204}Pb/^{206}Pb$. The Pb isotopic data of galena grains from the clay layer (BAX3.1160) are plotted in Figure 5. For comparison, the Pb data of secondary U minerals from the sandstone layer beneath the RZ (BAX3.1215 to 1290) are also plotted in the same figure. The Pb isotopic data points of individual minerals including galena measured in this study are plotted on the same single line. The Pb data of the secondary U minerals plotted on the single line can be explained by two-component mixing between the 2.05-Ga-old original uraninite and the reactor material including fissiogenic isotopes (Hidaka et al., 2005). Uraninite and U-rich goethite from the BAX3.1290 sandstone showed normal U isotopic compositions ($^{235}U/^{238}U$=0.00725) and higher $^{207}Pb^*/^{206}Pb^*$ ratios (0.126 to 0.128) corresponding to those 2.05 Ga, which represent the older original minerals as an end-member of the two-component mixing model. The data suggest that Pb in secondary U minerals was derived from uraninite with normal isotopic composition and not from the fissioned uraninite. All of the Pb data points of the galena measured in this study are close to

those of the 2.05-Ga-old original minerals. The Pb data suggest that the galena grains in the clay were also formed by the mixing of the two components during a recent alteration, and that a significant amount of Pb was derived from 2.05-Ga-old original uraninite rather than reactor uraninite.

3.3. Isotopic characterization of zircon

3.3.1. U and REE isotopes

The seven zircon grains found in the BAX03.1190 sample show a wide range of U content from 270 to 2.83×10^5 ppm. BSE images of the zircon grains are shown in Fig. 3(F). Two grains, numbered zircon 1 and 5, partly remain in a euhedral shape with an oscillatory zonal structure, and include numerous fractures. REE and U isotopic data of the zircon grains are summarized in Table 3. Although the U-rich region of individual zircon grains shows a normal $^{235}U/^{238}U$ ratio (=0.00725) within analytical uncertainties, it includes fissiogenic REE. Uraninite found in the sandstone (BAX03.1290) also has normal $^{235}U/^{238}U$ ratios and REE isotopic anomalies (Hidaka et al., 2005), suggesting the occurrence of chemical fractionation between REE and U during the recrystallization of secondary U minerals. The depleted U from the RZ was partially dissolved and mixed with a large amount of normal U from non reactor materials

3.3.2. U-Pb chronological interpretation

In-situ U-Pb dating of detrital zircon grains helps us to understand the thermal history of the sediments. However, as described in the previous section, the zircon crystals in this study include numerous high-U regions in micro-scale. Generally, it is

difficult to determine an accurate $^{206}Pb/^{238}U$ ratio for high-U zircon from *in-situ* isotopic analysis because of the inaccurate U-Pb calibration between the standard material and the analyzed samples (Williams and Hergt, 2000). The conventional U-Pb calibration technique is not appropriate for high-U zircon, because high-U zircon might have a different chemical composition from the standard zircon. Williams and Hergt (2000) studied the relationship between the SHRIMP U/Pb ages and the U contents of zircon, and revealed that the calibrated $^{206}Pb/^{238}U$ data increases as a function of U content over 2500 ppm. Therefore, in this study, only four analytical data with U concentrations of less than 2500 ppm (zircon 1-1, 1-3, 2-2, 3-4 in Fig. 3(F)) were selected from thirteen analytical spots, and used as reliably calibrated SHRIMP U-Pb data. In addition, the $^{206}Pb/^{238}U$ ratios of the other nine analytical spots with high-U contents (zircon 1-2, 1-4, 1-5, 3-3, 3-4, 4-5, 5-1, 5-2 and 7-1 in Fig. 3(F)) were determined from the analytical combination of U/Pb elemental ratios obtained by EPMA and Pb isotopic compositions obtained by SHRIMP. Although the U contents of zircon 1-2, 1-4 and 1-5 were less than 2500 ppm, SHRIMP analysis could not provide good statistics. Therefore, the three sets of data were collected from EPMA analysis. The U contents from eleven analytical spots (zircon 3-1, 3-2, 4-1, 4-2, 4-3, 4-4, 5-3, 6-1, 6-2, 6-3, 7-2), showing more than 2500 ppm by SHRIMP analysis, were not determined by EPMA, because the analytical regions in the grains were partly damaged after several SHRIMP analyses. Therefore, the thirteen data sets from twenty four analytical spots are used for further discussion.

Figure 6 shows a Tera-Wasserburg Concordia diagram. All of data from the thirteen analytical spots from the six zircon grains are listed in Table 4. If U-Pb decay system works as a chronometer, we can generally discuss geochronological history of the

sample from the data points of $^{238}U/^{206}Pb$ and $^{207}Pb/^{206}Pb$ on a Concordia diagram. However, in this case, in spite of the large variation of the $^{238}U/^{206}Pb$ data from 0.2 to 18, the $^{207}Pb/^{206}Pb$ ratios show a small variation except for two data points (0.1924 from zircon 1-1, and 0.1387 from zircon 2-2). The result suggests the existence of independent U and Pb sources that have migrated into zircon. Judging from the $^{207}Pb/^{206}Pb$ ratios (=0.115 to 0.126) commonly observed especially in the low-U/Pb parts of the zircon, the migrated Pb into the zircon was probably derived from the same source as that which formed the galena. In Fig. 5, the Pb isotopic data of the zircon are plotted in the same region of those of the galena. Furthermore, high $^{238}U/^{206}Pb$ points such as the analytical spots 5-1 and 5-2 show slightly higher $^{207}Pb/^{206}Pb$ ratios (0.122 to 0.126) than the other points ($^{207}Pb/^{206}Pb<0.12$), which also supports the incomplete mixing of independent Pb and U sources in this system. Previous Pb isotopic studies of U- and REE-bearing minerals in the sandstones beneath the Bangombé RZ show that a large mobilization of Pb, U and fissiogenic isotopes occurred by dolerite dyke intrusion (~0.8 Ga ago), and that the secondary minerals were formed by mixing between 2.05-Ga-old original minerals (non depleted U) and reactor materials (depleted U) during a recent alteration (Hidaka et al., 2005). The similarity of the Pb isotopic compositions suggests that the additional Pb and U fractions in the altered part of the zircon in the clay originated from the same sources as those of the secondary minerals in the sandstones.

The U-Pb data from the analytical spots 1-1, 2-1 and 2-2 are different from the others, suggesting chronological information on the old igneous activity associated with the basement rock formation. The three data points appear to form a single line with a different trend from the other ten data points. The U-Pb diagram in Fig. 6 suggests

that the U-Pb system of the inherited zircon was also disturbed by the mixing of the materials having $^{207}Pb/^{206}Pb$~0.12 with a low U content ($^{238}U/^{206}Pb<0.5$). As shown in Fig. 6, the intercept of the U-Pb Concordia and the single line consisting of the three data points gives a U-Pb age of 2.80 Ga, probably corresponding to the formation age of the basement rocks. Mathieu et al. (2001) reported an age of 2.87 Ga from the SHRIMP U-Pb analyses of two zircon crystals in the basement rocks. Ages of 2.7 to 2.9 Ga are reported for U-Th-Pb chemical ages of 6 of the 79 monazite crystals found in the FA sandstones and conglomerates (Montel et al., 1996). Therefore, it is reasonable to consider that the two zircon crystals are detrital materials derived from the basement in this site.

4. Conclusions

The isotopic data using a SHRIMP clearly show the distribution patterns of the fissiogenic REE isotopes from the RZ to the peripheral rocks. The isotopic variations of fissiogenic REE in the clay layer are much larger than those in the sandstone and black shales. The variations of the isotopic ratios of REE drastically change in the clay, while the isotopic ratios gradually change with the distance from the reactor in the sandstone. Our data demonstrate the important role of clays in effectively adsorbing the fission products released from the RZ.

The zircon crystals in the clays heterogeneously contain a U-rich region (up to 28.3 wt.%) with normal $^{235}U/^{238}U$ ratios (=0.00725) and significant amounts of fissiogenic REE, which indicate the migration of U-rich fluid in the grain. Although crystalline zircon is generally considered to be durable under most geochemical conditions, highly damaged zircon in this study showed significant migration of U and

REE.

From the Pb-Pb data of galena, it is interpreted that the galena grains in the clay were also formed by the mixing of the two components during a recent alteration, and that the significant amount of Pb was derived from 2.05-Ga-old original uraninite rather than reactor uraninite. The U-Pb systematics of zircon provides chronological information on the old igneous activity associated with the basement rock formation at 2.8 Ga and geochemical evidence of the incomplete mixing of independent Pb and U sources.

Acknowledgments

A part of this study was financially supported by a Grant-in-Aid for Scientific Research from the Japan Society for the Promotion of Science (to H.H., No. 17204051). We are grateful to J. Janeczek and A. Meshik for their critical reviews of this manuscript.

References

Bros, R., Hidaka, H., Kamei, G., Ohnuki, T., 2003. Mobilization and mechanisms of retardation in the Oklo natural reactor zone 2 (Gabon): Inferences from U, REE, Zr, Mo and Se isotopes. *Appl. Geochem.* **18,** 1807-1824.

Dymkov, Y., Holliger P., Pagel, M., Gorshukov, A., Artyukhina, A., 1997. Characterisation of a La-Ce-Sr-aluminous hydroxyl phosphate in nuclear zone 13 in the Oklo uranium deposit (Gabon). *Miner. Depos*. **32,** 617-620.

Evins, L.Z., Jensen, K.A., Ewing, R.C., 2005. Uraninite recrystallization and Pb loss in the Oklo and Bangombé natural fission reactors, Gabon. *Geochim. Cosmochim. Acta* **69,** 1589-1606.

Gancarz, A.J., 1978. U-Pb age ($2.05X10^9$ years) of the Oklo uranium deposit. Les Reacteurs de Fission Naturels. IAEA, Vienne, pp.513-520, TC-119/40.

Gauthier-Lafaye, F., Holliger, P., Blanc, P.-L., 1996. Natural fission reactors in the Franceville basin, Gabon: A review of the conditions and results of a "critical event" in a geologic system. *Geochim. Cosmochim. Acta* **60,** 4831-4852.

Gauthier-Lafaye F., Stille P. and Bros R, 2004. Special cases of natural analogues: The Gabon and Cigar lake U ore deposits. Gieré, R. & Stille, P. (eds) 2004. *Energy, Waste, and the Environment: A Geochemical Perspectives*. Geological Society, London, Special Publication, 236, 123-134.

Hidaka, H., Masuda, A., 1988. Nuclide analyses of rare earth elements of the Oklo uranium ore samples: A new method to estimate the neutron fluence. *Earth Planet. Sci. Lett.* **88,** 330-336.

Hidaka, H., Holliger, P., 1998. Geochemical and neutronic characteristics of the natural fossil fission reactors at Oklo and Bangombé, Gabon. *Geochim. Cosmochim. Acta* **62,** 89-108.

Hidaka, H., Gauthier-Lafaye, F., 2000. Redistribution of fissiogenic and non-fissiogenic REE, Th and U in and around natural fission reactors at Oklo and

Bangombé, Gabon. *Geochim. Cosmochim. Acta* **64,** 2093-2108.

Hidaka, H., Janeczek, J., Skomurski, F.N., Ewing, R., Gauthier-Lafaye, F., 2005. Geochemical fixation of rare earth elements into secondary minerals in sandstones beneath a natural fission reactor at Bangombé, Gabon. *Geochim. Cosmochim. Acta* **69,** 685-694.

Holliger, P., 1988. Ages U/Pb defines in situ sur oxides d'uranium a l'analyseur ionique: methodologie et consequences geochimiques. *C. R. Acad. Sci. Paris* **307,** 367-373.

Horie, K., Hidaka, H., Gauthier-Lafaye, F., 2004. Isotopic evidence for trapped fissiogenic REE and nucleogenic Pu in apatite and Pb evolution at the Oklo natural reactor. *Geochim. Cosmochim. Acta* **68,** 115-125.

Janeczek, J., Ewing, R., 1996a. Phosphatian coffinite with rare earth elements and Ce-rich françoisite from sandstone beneath a natural fission reactor at Bangombé, Gabon. *Mineral. Mag.* **60,** 665-669.

Janeczek, J., Ewing, R., 1996b. Florencite-(La) with fissiogenic REEs from a natural fission reactor at Bangombé, Gabon. *Am. Mineral.* **81,** 1263-1269.

Jensen, K.A., Ewing, R.C., 2001. The Okélobondo natural fission reactor, southeast Gabon: geology, mineralogy and retardation of nuclear reaction products. *Geol. Soc. Am. Bull.* **113/1,** 32-62.

Mathieu, R., Zetterström, L., Cuney, M., Gauthier-Lafaye, F., Hidaka, H., 2001. Alteration of monazite and zircon and lead migration as geochemical tracers of fluid paleocirculations around the Oklo-Okélobondo and Bamgombé natural nuclear reaction zones (Franceville basin, Gabon). *Chem. Geol.* **171,** 147-171.

Montel, J.M., Foret, S., Veschambre, M., Nicollet, C., Provost, A., 1996. Electron microprobe dating of monazite. *Chem. Geol.* **131,** 37-53.

Paces, J. B., Miller, J. D., 1993. Precise U-Pb age of Duluth Complex and related mafic intrusions, northeastern Minnesota: Geochronological insights into physical,

petrogenic, paleomagnetic and tectonomagmatic processes associated with the 1.1 Ga midcontinent rift system. *J. Geophys.Res.* **98,** 13997-14013.

Ruffenach, J.C., 1979. Les reacteurs naturels d'Oklo: parametres neutroniques, date et duree de fonctionnement, migration de l'uranium et des produits de fission. Thesis, Univ. Paris VII, 350 pp.

Stille, P., Gauthier-Lafaye, F., Jensen, K.A., Salah, S., Bracke, G., Ewing, R.C., Louvat, D., Million, D., 2003. REE mobility in groundwater proximate to the natural fission reactor at Bangombé (Gabon). *Chem. Geol.* **198,** 289-304.

Williams, I.S., Hergt, J.M., 2000. U-Pb dating of Tasmanian dolerite: A cautionary tale of SHRIMP analysis of high-U zircon. In: J.D. Woodhead, J.M. Hergt, W.P. Noble eds. Beyond 2000: New Frontiers in Isotope Geoscience, Lorne, Abstract and Proceedings.

Figure captions

Figure 1. Geological setting of the Bangombé area. (A) Geological map of the Franceville basin. (B) Locations of the Bangombé RZ and the boreholes. Three boreholes, BA145, BAX3 and BAX8, intersect the RZ.

Figure 2. Petrologic type of stratigraphic section of the BAX3 drill core and the locations of samples used in this study. BAX3.1170 is from the clay part. BAX3.1040 and 1065 are from black shales.

Figure 3. BSE images of typical micro-minerals measured in this study. (A) to (C): Coffinite. (D): Coffinite with a rim of a few μm of françoisite. (E): galena with U-rich inclusions. (F): zircon crystals. The circles and the numbers in the photos reveal analytical spots that correspond to the isotopic data in Tables 1, 3 and 4. Individual scale bars in the photos are 50 μm.

Figure 4. Depth-dependent variations of $^{140}Ce/^{142}Ce$, $^{145}Nd/^{146}Nd$, $^{149}Sm/^{147}Sm$ and $^{153}Eu/^{151}Eu$ isotopic ratios of U- and REE-bearing minerals in the BAX3 drill core. The vertical axis indicates the depth from the surface in meters. The data points with solid squars (micro-uraninite in BAX3.1040 and 1065), solid triangles (coffinite in BAX3.1170), and open triangles (U-inclusion in BAX3.1170) are from this study. The data points with open squars (uraninite in BAX3.1180), open circle (florencite in BAX3.1175), and open diamonds (U- and REE-bearing minerals in BAX3.1225, 1240 and 1290) are from previous works (Hidaka and Gauthier-Lafaye, 2000; Janeczek and Ewing, 1996b; Hidaka et al., 2005).

Figure 5. $^{204}Pb/^{206}Pb$ vs. $^{207}Pb/^{206}Pb$ diagram of galena grains from the clay (BAX3.1160) above the Bangombé reactor. The data points with solid circles are from this study, and those with open circles are from U- and REE-bearing minerals in sandstone samples (BAX3.1215, 1225, 1240 and 1290) beneath the reactor by Hidaka et al. (2005).

Figure 6. Tera-Wasserburg U-Pb Concordia diagram of six zircon grains from the clay

(BAX3.1160) above the Bangombé reactor. The data points with solid circles are from SHRIMP analyses, and those with open circles are from the combination of SHRIMP and EPMA analyses (see text).

Figure 1. Kikuchi et al.

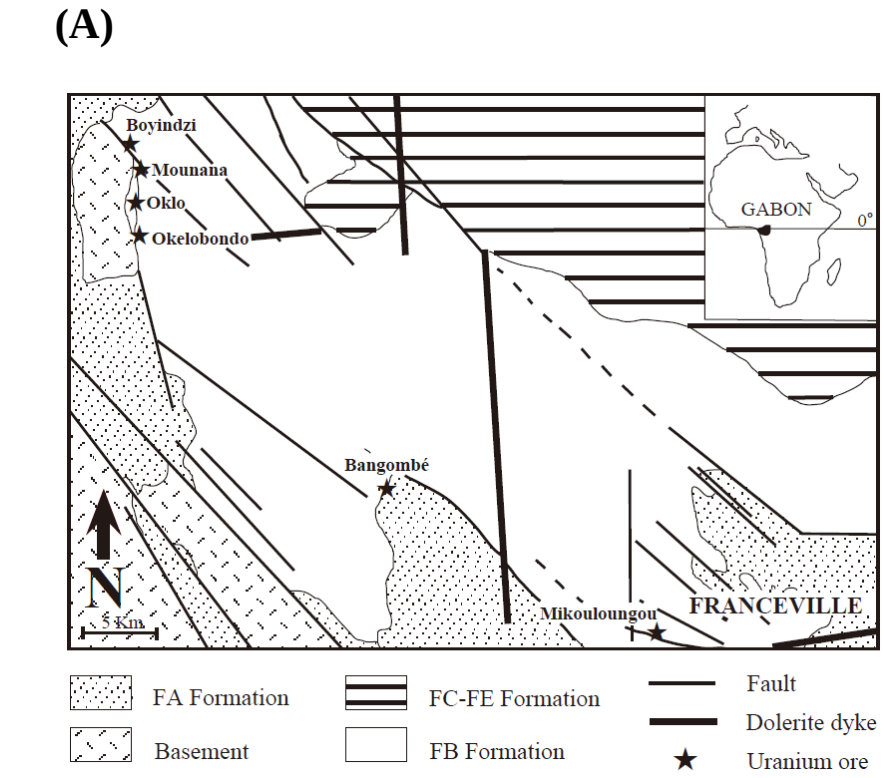

Figure 2. Kikuchi et al.

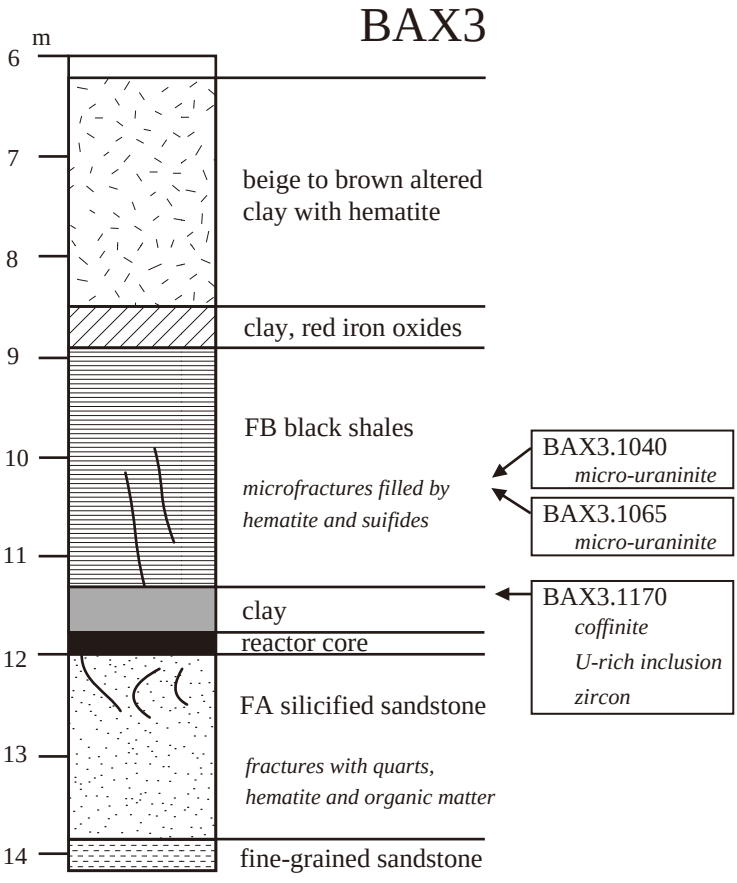

(A) coffinite-1

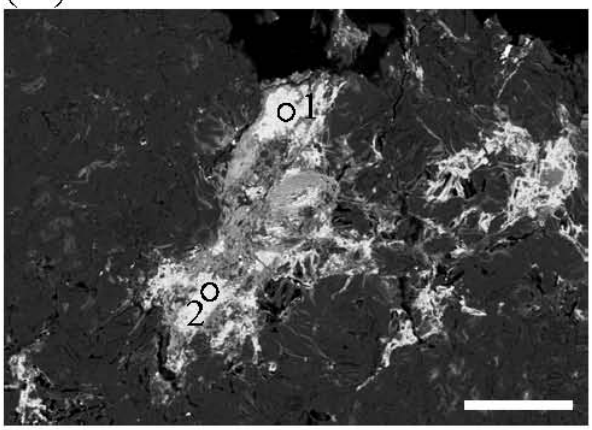

(B) coffinite-2

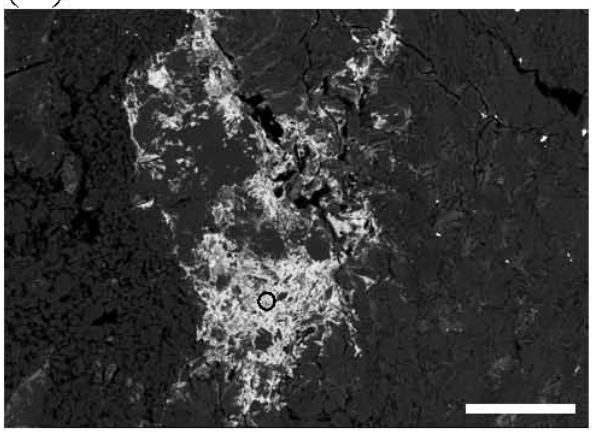

(C) coffinite-3

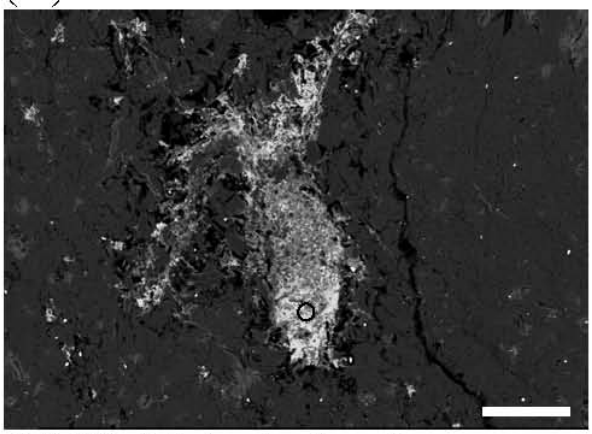

(D) coffinite-4

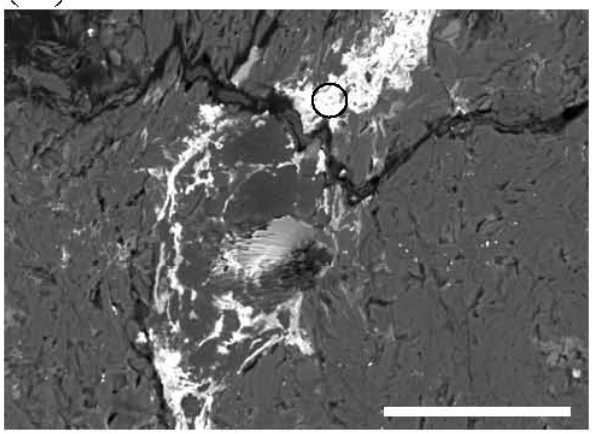

(E) U-rich inclusion-1

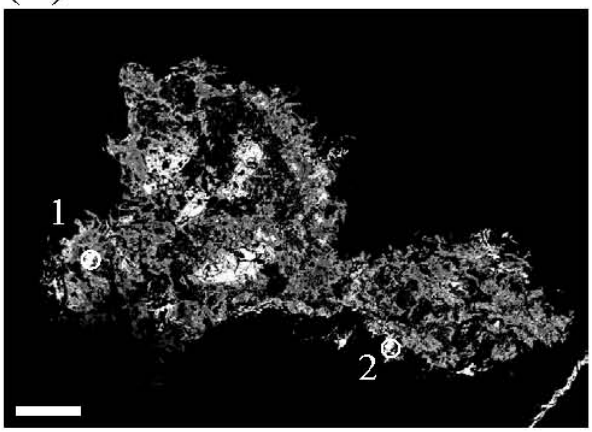

(F) zircon

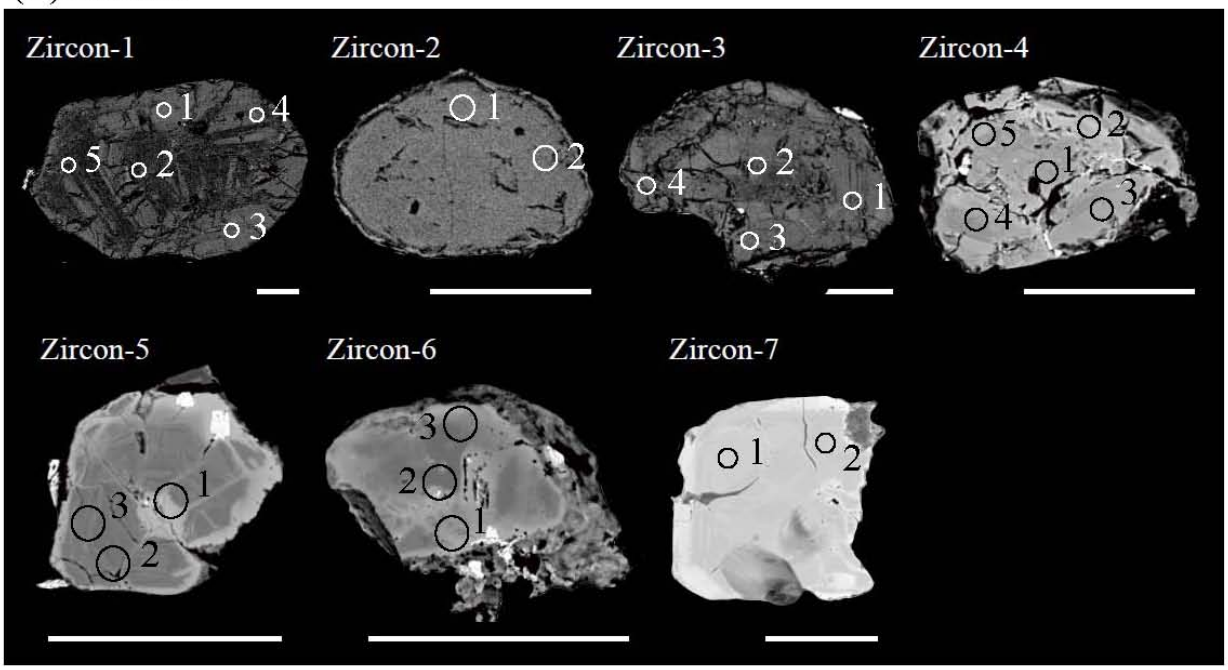
Zircon-1
1
4
5
2
3
Zircon-2
1
2
Zircon-3
4
2
1
3
Zircon-4
5
2
1
3
4
Zircon-5
3
1
2
Zircon-6
3
2
1
Zircon-7
1
2

Figure 4. Kikuchi et al.

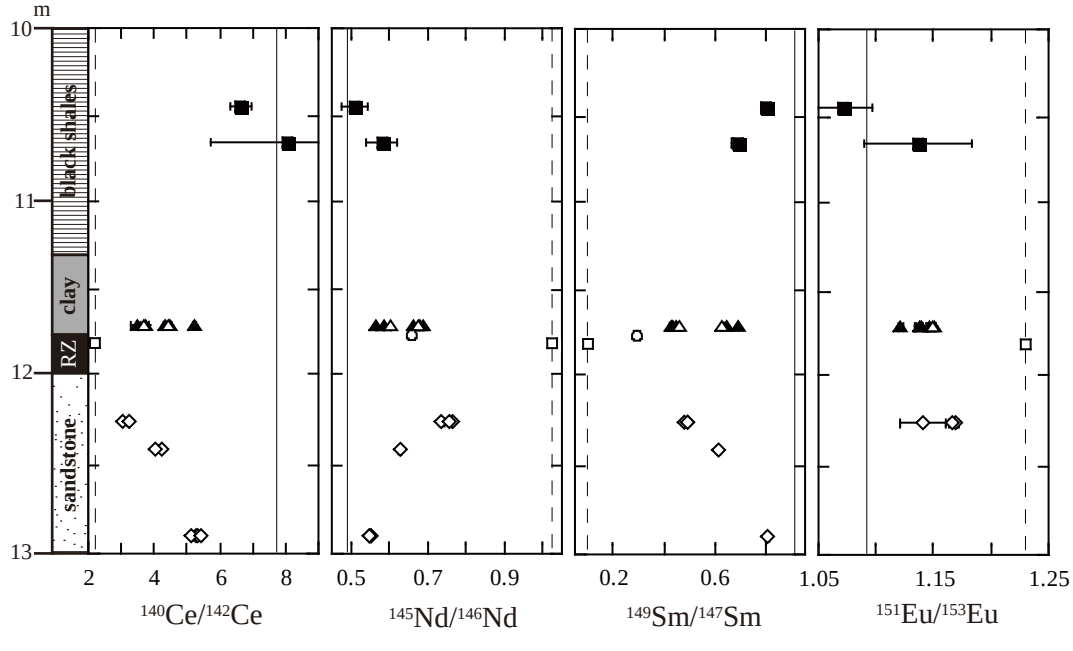

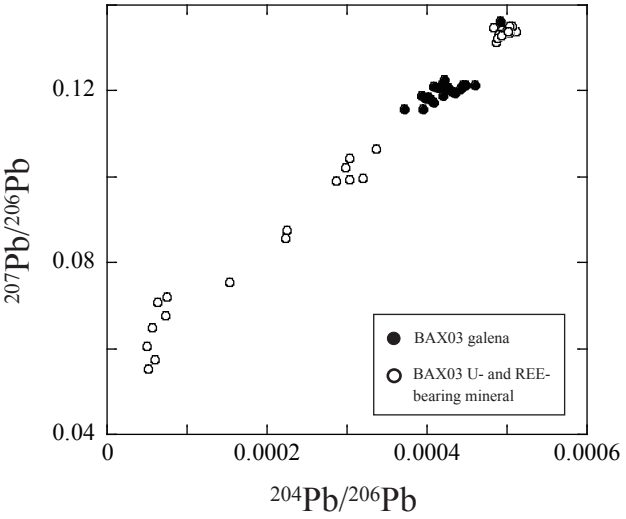
0.12
0.08
0.04
0
0.0002
0.0004
0.0006
$^{207}Pb/^{206}Pb$
$^{204}Pb/^{206}Pb$
BAX03 galena
BAX03 U- and REE-bearing mineral

Fig. 6 Kikuchi et al.

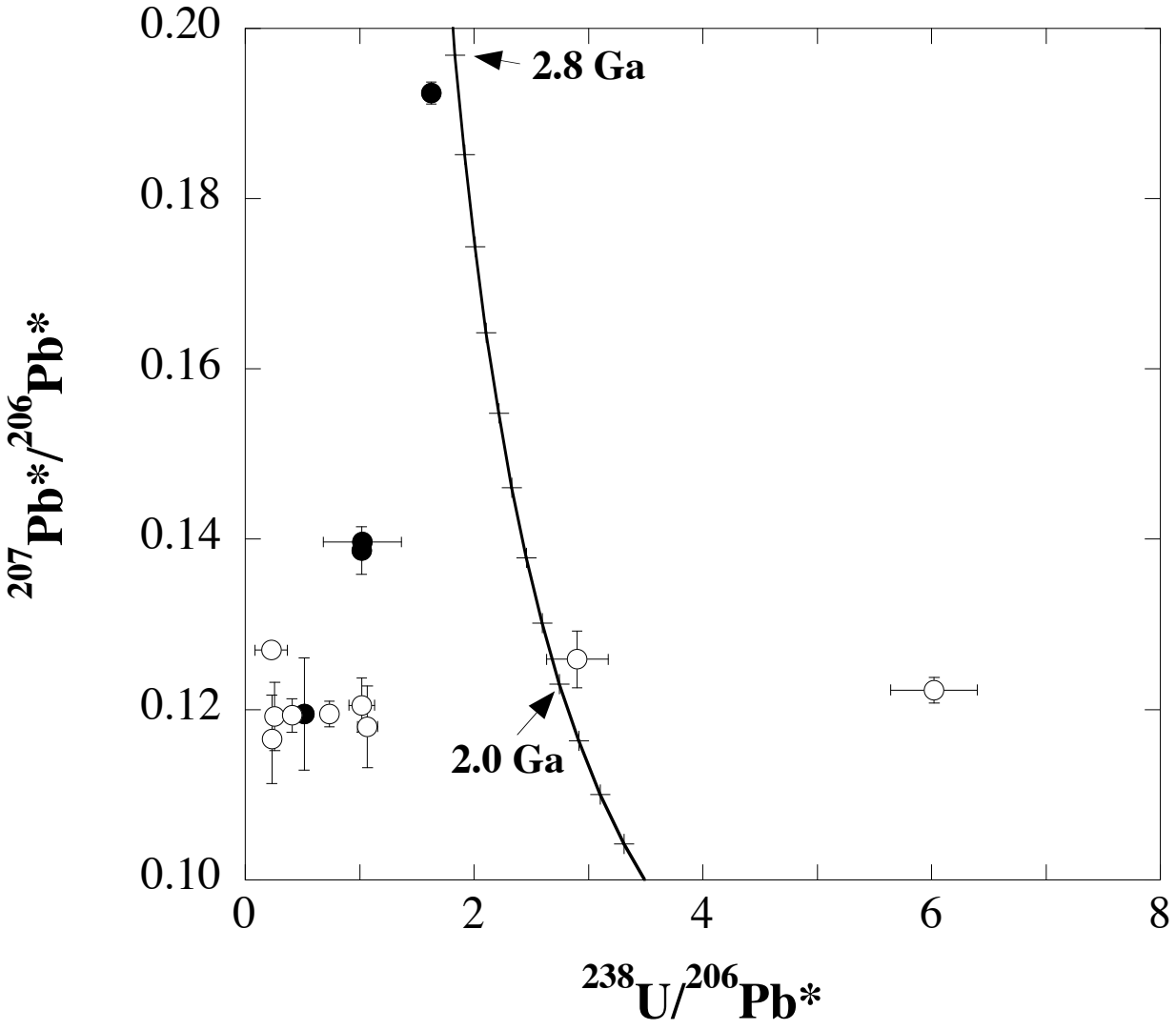

Table 1. REE isotopic ratios of micro-minerals by SHRIMP analyses

(A) Ce, Nd, Sm and Eu isotopic ratios

	$^{140}Ce/^{142}Ce$	$^{143}Nd/^{146}Nd$	$^{145}Nd/^{146}Nd$	$^{149}Sm/^{147}Sm$	$^{153}Eu/^{151}Eu$
BAX3.1040					
micro-uraninite	6.64 ± 0.33	0.682 ± 0.038	0.581 ± 0.041	0.796 ± 0.003	1.07 ± 0.03
BAX3.1065					
micro-uraninite	8.07 ± 2.36	0.513 ± 0.056	0.509 ± 0.034	0.688 ± 0.022	1.14 ± 0.05
BAX3.1170					
coffinite-1-1	4.31 ± 0.04	0.875 ± 0.002	0.585 ± 0.001	0.641 ± 0.002	1.137 ± 0.003
coffinite-1-2	4.49 ± 0.04	0.846 ± 0.002	0.566 ± 0.001	0.687 ± 0.001	1.121 ± 0.002
coffinite-2	3.76 ± 0.07	1.028 ± 0.003	0.689 ± 0.001	0.425 ± 0.001	1.151 ± 0.001
coffinite-3	3.51 ± 0.23	1.017 ± 0.006	0.681 ± 0.001	0.447 ± 0.001	1.147 ± 0.001
coffinite-4	5.25 ± 0.05	0.983 ± 0.002	0.663 ± 0.001	0.431 ± 0.001	1.139 ± 0.004
U-rich inclusion1-1	3.71 ± 0.13	0.966 ± 0.002	0.677 ± 0.002	0.457 ± 0.002	1.149 ± 0.002
U-rich inclusion1-2	4.43 ± 0.06	0.893 ± 0.001	0.603 ± 0.002	0.627 ± 0.003	Not analyze
BAX3.1180					
uraninite*	2.209	1.464	1.025	0.101	1.23
STD					
NIST610	7.73 ± 0.03	0.735 ± 0.001	0.490 ± 0.001	0.906 ± 0.002	1.092 ± 0.002

Analytical uncertainties are 1σ of the mean.

*The data are from Hidaka and Gauthier-Lafaye (2000).

Table 1. continued

(B) Gd isotopic ratios

	$^{155}Gd/^{160}Gd$	$^{156}Gd/^{160}Gd$	$^{157}Gd/^{160}Gd$	$^{158}Gd/^{160}Gd$	$(^{155}Gd+^{156}Gd)/^{160}Gd$	$(^{157}Gd+^{158}Gd)/^{160}Gd$
BAX3.1170						
coffinite-1-1	0.695 ± 0.05	0.993 ± 0.007	0.700 ± 0.003	1.194 ± 0.004	1.688 ± 0.012	1.894 ± 0.006
coffinite-1-2	0.678 ± 0.07	1.008 ± 0.007	0.706 ± 0.006	1.178 ± 0.006	1.685 ± 0.013	1.883 ± 0.011
coffinite-2	0.710 ± 0.02	0.961 ± 0.003	0.726 ± 0.002	1.139 ± 0.003	1.671 ± 0.004	1.864 ± 0.005
coffinite-3	0.683 ± 0.03	1.030 ± 0.003	0.688 ± 0.003	1.198 ± 0.003	1.712 ± 0.005	1.886 ± 0.005
coffinite-4	0.709 ± 0.08	1.065 ± 0.003	0.707 ± 0.006	1.211 ± 0.008	1.774 ± 0.021	1.917 ± 0.014
U-rich inclusion-1-2	0.732 ± 0.01	1.053 ± 0.011	0.713 ± 0.008	1.200 ± 0.010	1.785 ± 0.022	1.913 ± 0.018
STD						
NIST610	0.710 ± 0.02	0.961 ± 0.005	0.726 ± 0.002	1.139 ± 0.005	1.671 ± 0.006	1.701 ± 0.007

Analytical uncertainties are 1σ of the mean.

The data of micro-uraninite from BAX3.1040 and 1065, and U-rich inclusion1-1 from BAX3.1170 were not obtained.

*The data are from Hidaka and Gauthier-Lafaye (2000).

Table 2. Pb isotopic data of galena in BAX3.1170

	^{204}Pb /^{206}Pb (x10^{-4})	^{207}Pb /^{206}Pb	^{208}Pb /^{206}Pb
galena 1-1	4.45 ± 0.05	0.1211 ± 0.0008	0.0197 ± 0.0002
galena 1-2	4.49 ± 0.04	0.1213 ± 0.0009	0.0195 ± 0.0002
galena 1-3	4.46 ± 0.07	0.1213 ± 0.0010	0.0196 ± 0.0002
galena 1-4	4.36 ± 0.03	0.1196 ± 0.0006	0.0193 ± 0.0001
galena 1-5	4.61 ± 0.03	0.1213 ± 0.0006	0.0202 ± 0.0001
galena 1-6	4.42 ± 0.04	0.1203 ± 0.0007	0.0192 ± 0.0001
galena 2-1	4.93 ± 0.11	0.1349 ± 0.0015	0.0216 ± 0.0002
galena 2-2	4.91 ± 0.10	0.1362 ± 0.0010	0.0225 ± 0.0002
galena 3-1	4.01 ± 0.10	0.1187 ± 0.0005	0.0176 ± 0.0002
galena 3-2	4.20 ± 0.06	0.1207 ± 0.0016	0.0184 ± 0.0002
galena 3-3	4.18 ± 0.06	0.1213 ± 0.0009	0.0190 ± 0.0002
galena 3-4	4.09 ± 0.13	0.1212 ± 0.0008	0.0191 ± 0.0003
galena 4-1	4.06 ± 0.12	0.1180 ± 0.0034	0.0170 ± 0.0005
galena 4-2	3.71 ± 0.08	0.1157 ± 0.0008	0.0175 ± 0.0002
galena 4-3	4.21 ± 0.04	0.1190 ± 0.0006	0.0189 ± 0.0001
galena 4-4	4.08 ± 0.10	0.1173 ± 0.0006	0.0183 ± 0.0002
galena 4-5	3.93 ± 0.07	0.1189 ± 0.0005	0.0183 ± 0.0002
galena 4-6	3.98 ± 0.08	0.1183 ± 0.0006	0.0179 ± 0.0002
galena 5-1	4.32 ± 0.10	0.1199 ± 0.0024	0.0187 ± 0.0003
galena 5-2	4.26 ± 0.15	0.1209 ± 0.0025	0.0196 ± 0.0005
galena 5-3	4.22 ± 0.07	0.1225 ± 0.0004	0.0193 ± 0.0001
galena 6-1	4.14 ± 0.06	0.1207 ± 0.0005	0.0188 ± 0.0001
galena 6-2	4.23 ± 0.05	0.1205 ± 0.0004	0.0189 ± 0.0001
galena 6-3	3.95 ± 0.16	0.1158 ± 0.0010	0.0184 ± 0.0003

Analytical uncertainties are 1σ of the mean.

Table 3. REE isotopic data of zircon in BAX3.1170

(A) Ce, Nd, Sm and Eu

	$^{140}Ce/^{142}Ce$	$^{143}Nd/^{146}Nd$	$^{145}Nd/^{146}Nd$	$^{149}Sm/^{147}Sm$	$^{153}Eu/^{151}Eu$
zircon 1-1	6.68 ± 0.19	0.819 ± 0.02	0.557 ± 0.001	0.765 ± 0.003	1.100 ± 0.006
zircon 1-2	6.07 ± 0.06	0.796 ± 0.02	0.537 ± 0.001	0.811 ± 0.003	1.112 ± 0.002
zircon 1-3	5.79 ± 0.01	0.803 ± 0.01	0.543 ± 0.001	0.790 ± 0.002	1.117 ± 0.003
zircon 1-4	6.09 ± 0.05	0.811 ± 0.01	0.551 ± 0.001	0.756 ± 0.001	1.122 ± 0.001
zircon 1-5	5.53 ± 0.05	0.815 ± 0.01	0.549 ± 0.001	0.752 ± 0.001	1.123 ± 0.002
zircon 2-2	4.92 ± 0.01	0.906 ± 0.01	0.614 ± 0.001	0.606 ± 0.002	1.112 ± 0.011
zircon 3-2	6.03 ± 0.06	0.793 ± 0.01	0.534 ± 0.001	0.808 ± 0.001	1.116 ± 0.002
zircon 3-4	5.97 ± 0.05	0.792 ± 0.01	0.533 ± 0.001	0.801 ± 0.001	1.103 ± 0.004
zircon 4-1	5.44 ± 0.06	0.836 ± 0.01	0.564 ± 0.001	0.699 ± 0.002	1.125 ± 0.002
zircon 5-1	4.27 ± 0.09	0.900 ± 0.03	0.604 ± 0.002	0.606 ± 0.003	1.173 ± 0.003
zircon 6-2	4.60 ± 0.80	0.911 ± 0.03	0.611 ± 0.002	0.573 ± 0.002	1.136 ± 0.001
zircon 7-1	5.05 ± 0.06	0.848 ± 0.02	0.568 ± 0.001	0.693 ± 0.002	1.126 ± 0.002
zircon 7-2	5.09 ± 0.07	0.846 ± 0.01	0.570 ± 0.001	0.673 ± 0.002	Not analyzed
STD					
NIST610	7.73 ± 0.03	0.735 ± 0.01	0.490 ± 0.001	0.906 ± 0.002	1.091 ± 0.001
AS3	7.55 ± 0.06	0.741 ± 0.01	0.484 ± 0.001	0.929 ± 0.001	1.073 ± 0.005

Analytical uncertainties are 1σ of the mean.

Table 3. continued

(B) Gd

	$^{155}Gd/^{160}Gd$	$^{156}Gd/^{160}Gd$	$^{157}Gd/^{160}Gd$	$^{158}Gd/^{160}Gd$	$(^{155}Gd+^{155}Gd)/^{160}Gd$	$(^{155}Gd+^{155}Gd)/^{160}Gd$
zircon 1-1	0.717 ± 0.009	0.994 ± 0.015	0.738 ± 0.009	1.196 ± 0.014	1.711 ± 0.024	1.934 ± 0.023
zircon 1-2	0.694 ± 0.003	0.985 ± 0.003	0.703 ± 0.003	1.175 ± 0.002	1.678 ± 0.005	1.877 ± 0.005
zircon 1-3	0.694 ± 0.004	0.985 ± 0.003	0.708 ± 0.002	1.176 ± 0.003	1.679 ± 0.006	1.885 ± 0.005
zircon 1-4	0.676 ± 0.002	0.980 ± 0.002	0.698 ± 0.001	1.178 ± 0.002	1.656 ± 0.003	1.875 ± 0.003
zircon 1-5	0.705 ± 0.003	0.982 ± 0.004	0.713 ± 0.003	1.168 ± 0.004	1.687 ± 0.007	1.881 ± 0.005
zircon 2-2	0.719 ± 0.010	0.897 ± 0.028	0.708 ± 0.011	1.208 ± 0.017	1.616 ± 0.028	1.916 ± 0.024
zircon 3-2	0.705 ± 0.003	0.991 ± 0.004	0.704 ± 0.003	1.182 ± 0.004	1.696 ± 0.006	1.886 ± 0.005
zircon 3-4	0.691 ± 0.005	0.979 ± 0.005	0.692 ± 0.005	1.171 ± 0.006	1.670 ± 0.006	1.863 ± 0.010
zircon 4-1	0.696 ± 0.003	1.002 ± 0.004	0.711 ± 0.003	1.191 ± 0.004	1.699 ± 0.006	1.902 ± 0.007
zircon 5-1	0.597 ± 0.007	0.949 ± 0.008	0.662 ± 0.004	1.174 ± 0.004	1.546 ± 0.012	1.837 ± 0.007
zircon 6-2	0.668 ± 0.002	0.976 ± 0.003	0.689 ± 0.001	1.181 ± 0.002	1.643 ± 0.004	1.869 ± 0.003
zircon 7-1	0.695 ± 0.004	0.974 ± 0.004	0.711 ± 0.004	1.156 ± 0.005	1.669 ± 0.004	1.867 ± 0.004
STD						
NIST610	0.710 ± 0.002	0.961 ± 0.005	0.726 ± 0.002	1.139 ± 0.005	1.671 ± 0.006	1.864 ± 0.007
AS3	0.696 ± 0.004	0.960 ± 0.005	0.735 ± 0.005	1.167 ± 0.006	1.656 ± 0.009	1.902 ± 0.010

Analytical uncertainties are 1σ of the mean.

Gd isotopic ratios of zircon 7-2 were not analyzed.

Table 4. U and Pb isotopic data and U contents of zircon in BAX3.1170

	$^{204}Pb/^{206}Pb$ ($x10^{-4}$)	$^{207}Pb/^{206}Pb$	$^{208}Pb/^{206}Pb$	$^{235}U/^{238}U$ ($x10^{-3}$)	U content (ppm)		$^{238}U/^{206}Pb$
					SHRIMP	EPMA	
zircon 1-1	0.07 ± 0.04	0.1924 ± 0.0013	0.1532 ± 0.0021	7.30 ± 0.08	297	Not analyzed	1.627 ± 0.043
zircon 1-2	4.23 ± 0.12	0.1192 ± 0.0040	0.0194 ± 0.0007	7.37 ± 0.18		874	0.259 ± 0.014
zircon 1-3	4.23 ± 0.22	0.1195 ± 0.0066	0.0274 ± 0.0015	7.33 ± 0.14	1760	Not analyzed	0.516 ± 0.043
zircon 1-4	4.37 ± 0.14	0.1205 ± 0.0032	0.0208 ± 0.0006	7.37 ± 0.16		88.1	1.020 ± 0.111
zircon 1-5	4.35 ± 0.11	0.1195 ± 0.0015	0.0198 ± 0.0003	7.34 ± 0.08		461	0.736 ± 0.043
zircon 2-1	3.65 ± 0.49	0.1397 ± 0.0006	0.0331 ± 0.0004	7.24 ± 0.11	393	Not analyzed	1.025 ± 0.339
zircon 2-2	3.46 ± 0.30	0.1387 ± 0.0028	0.0308 ± 0.0008	Not analyzed	271	Not analyzed	1.018 ± 0.053
zircon 3-1	4.51 ± 0.52	0.1073 ± 0.0160	0.0176 ± 0.0026	Not analyzed	>2500	Not analyzed	
zircon 3-2	4.28 ± 0.33	0.1148 ± 0.0035	0.0336 ± 0.0011	7.34 ± 0.06	>2500	Not analyzed	
zircon 3-3	4.26 ± 0.21	0.1180 ± 0.0048	0.0260 ± 0.0013	Not analyzed	>2500	$3.36x10^3$	1.070 ± 0.089
zircon 3-4	4.15 ± 0.29	0.1165 ± 0.0052	0.0185 ± 0.0008	7.32 ± 0.06	143	Not analyzed	0.233 ± 0.024
zircon 4-1	4.25 ± 0.11	0.1226 ± 0.0034	0.0196 ± 0.0005	7.26 ± 0.04	>2500	Not analyzed	
zircon 4-2	4.42 ± 0.13	0.1202 ± 0.0006	0.0190 ± 0.0001	Not analyzed	>2500	Not analyzed	
zircon 4-3	3.84 ± 0.47	0.1141 ± 0.0047	0.0182 ± 0.0008	7.30 ± 0.08	>2500	Not analyzed	
zircon 4-4	4.50 ± 0.10	0.1199 ± 0.0019	0.0191 ± 0.0003	Not analyzed	>2500	Not analyzed	
zircon 4-5	4.33 ± 0.09	0.1193 ± 0.0020	0.0190 ± 0.0004	Not analyzed	>2500	$7.69x10^3$	0.410 ± 0.010
zircon 5-1	4.51 ± 0.15	0.1259 ± 0.0033	0.0206 ± 0.0005	7.30 ± 0.12	>2500	$2.49x10^5$	2.903 ± 0.269
zircon 5-2	4.04 ± 0.67	0.1223 ± 0.0015	0.0202 ± 0.0005	7.27 ± 0.08	>2500	$7.42x10^3$	6.024 ± 0.379
zircon 5-3	4.35 ± 0.35	0.1248 ± 0.0044	0.0182 ± 0.0006	Not analyzed	>2500	Not analyzed	
zircon 6-1	4.27 ± 0.17	0.1223 ± 0.0014	0.0195 ± 0.0003	Not analyzed	>2500	Not analyzed	
zircon 6-2	4.60 ± 0.20	0.1213 ± 0.0047	0.0187 ± 0.0009	7.26 ± 0.08	>2500	Not analyzed	
zircon 6-3	4.86 ± 0.20	0.1220 ± 0.0039	0.0192 ± 0.0007	Not analyzed	>2500	Not analyzed	
zircon 7-1	4.24 ± 0.20	0.1270 ± 0.0005	0.0293 ± 0.0003	7.31 ± 0.08	>2500	$2.69x10^4$	0.229 ± 0.142
zircon 7-2	4.16 ± 0.16	0.1237 ± 0.0007	0.0233 ± 0.0002	7.38 ± 0.04	>2500	Not analyzed	

Analytical uncertainties are 1σ of the mean.